Reprinted from

JAPANESE JOURNAL OF
APPLIED
PHYSICS

REGULAR PAPER

One Dimensional Modeling of Radio Frequency Electric Field Penetration into Magnetized Plasmas

Takeshi Matsuoka, Timofei S. Rudenko, Ikkoh Funaki, Konstantin P. Shamrai, Takahiro Nakamura, Hiroyuki Nishida, Takao Tanikawa, Tohru Hada, and Shunjiro Shinohara

Jpn. J. Appl. Phys. **51** (2012) 096201

Japanese Journal of Applied Physics **51** (2012) 096201 **REGULAR PAPER**
http://dx.doi.org/**10.1143/JJAP.51.096201**

One Dimensional Modeling of Radio Frequency Electric Field Penetration into Magnetized Plasmas

Takeshi Matsuoka[1]*, Timofei S. Rudenko[2], Ikkoh Funaki[1], Konstantin P. Shamrai[2], Takahiro Nakamura[3], Hiroyuki Nishida[4], Takao Tanikawa[5], Tohru Hada[6], and Shunjiro Shinohara[4]

[1]*Japan Aerospace Exploration Agency, Sagamihara 252-5210, Japan*
[2]*Institute for Nuclear Research, National Academy of Sciences of Ukraine, Kiev 03680, Ukraine*
[3]*Graduate School of Engineering, Tokyo University of Agriculture and Technology, Koganei, Tokyo 184-8588, Japan*
[4]*Institute of Engineering, Tokyo University of Agriculture and Technology, Koganei, Tokyo 184-8588, Japan*
[5]*Research Institute of Science and Technology, Tokai University, Hiratsuka, Kanagawa 259-1292, Japan*
[6]*Interdisciplinary Graduate School of Engineering Sciences, Kyushu University, Kasuga, Fukuoka 816-8580, Japan*

Received March 9, 2012; revised May 7, 2012; accepted June 3, 2012; published online August 20, 2012

Full penetration of RF electric fields into magnetized plasmas is expected in order to realize the Lissajous helicon plasma accelerator (LHPA). We study the electric field penetration in bulk plasma in one-dimensional electrostatic approximation using two analytical models: the matrix sheath model and the vacuum gap model. An identical formula for the electric field is obtained from the models. The formula is benchmarked by particle-in-cell (PIC) simulations. The full penetration of the electric field is realized when the relation ($q \ll 0.01$) is satisfied, where q is the measure of the degree of the shielding effect due to plasma density and electron magnetization. © 2012 The Japan Society of Applied Physics

1. Introduction

Electric propulsion[1,2] in space applications has been used to save the amount of propellants owing to its high specific impulses, which reduce the cost or time for various space missions. Successful thrusters such as ion or Hall thrusters have a lifetime which is limited by two factors whichever shorter one: erosion of electrodes and the lifetime of charge neutralizers (hollow cathodes).[3,4] Therefore, removing the electrode and the neutralizer enables the extension of the lifetime of the thruster. Several schemes are proposed for electrodeless thrusters with helicon plasma sources that can produce high-density plasmas over a wide range of operating parameters.[5–7] One of the electrodeless thrusters is the Lissajous helicon plasma accelerator (LHPA),[8–12] in which the thrust is produced by the electromagnetic force (Lorentz force). Two other helicon plasma-based electrodeless thrusters use magnetic nozzle (VASIMR[13]) and static electric field (double layer[14]) acceleration.

Figure 1 shows a configuration of the Lissajous acceleration.[8–12] Plasma is generated and accelerated inside the dielectric tube by RF antennas outside the tube, therefore, there is no contact between the electrodes and the plasma. Plasma is generated by a helicon source (not shown in the figure) in a magnetic field that is produced by a solenoid coil whose axis is in the z direction. Then the plasma is transported along the z direction by the axial magnetic field, as indicated by a thick gray arrow in Fig. 1. The thrust is produced by the Lorentz force, which is the product of azimuthal current (j_θ) and the radial magnetic field ($j_\theta \times B_r$) near the end of the solenoid. A key issue is how to produce the azimuthal current.

The use of a rotating electric field (REF) is proposed to excite the azimuthal current in the Lissajous acceleration. The transverse REF vector $E_\perp$, which rotates at a driving frequency of ω around the z-axis, is generated by two sets of planar antennas. Those antennas are connected to RF power supplies, as shown in Fig. 1. Selection of the applied frequency in a range specified by ω_{LH} (lower hybrid frequency) $\ll \omega \ll \omega_{ce}$ (electron cyclotron frequency) implies

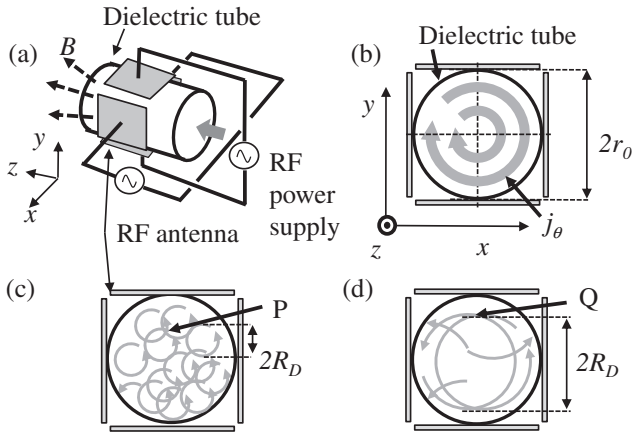

Fig. 1. (a) Configuration of the Lissajous acceleration. (b) Cross-sectional view of the thruster with j_θ. (c) Cross-sectional view of the thruster in x–y plane with individual electron trajectories for $R_D/r_0 \ll 1$ and (d) $R_D/r_0 \sim 1$.

immobile ions. Therefore, we consider electron current for j_θ. Figure 1(b) shows a cross-sectional plane of the thruster. It can be shown that the guiding center of a single electron shows $E \times B$ drift motion in a circular trajectory whose radius is $R_D = E_\perp/\omega B_z$.[8–12] Here, B_z is the axial component of the magnetic field. This electron drift is a source of j_θ.[11,12] In Figs. 1(c) and 1(d), gray circles indicate the trajectories of the guiding center for individual electrons. The azimuthal current is found to be proportional to R_D/r_0 by integration of individual electron motions in radially inhomogeneous plasma whose density peaks on the z-axis.[11,12] In fact, a series of two dimensional PIC simulations showed that j_θ is proportional to R_D/r_0 up to an optimum ratio of ~0.4 then decreases after reaching this optimum value.[12] The rise and fall of j_θ can be understood qualitatively from Figs. 1(c) and 1(d). For $R_D/r_0 \ll 1$, as shown in Fig. 1(c), the direction of electron velocity at point P in the figure is random. Therefore, the contribution from each electron to j_θ cancels out. However, for $R_D/r_0 \sim 1$, the degree of cancelation at point Q is small. The difference in the degree of the "cancelation effect" is accounted by R_D/r_0 and is responsible for the rise of j_θ. Whereas, the fall of j_θ can be

*E-mail address: takeshi.matsuoka1@gd.isas.jaxa.jp

explained by particle loss to the dielectric tube wall. The number of trajectories that intercept the wall is larger for $R_D/r_0 \sim 1$ than for $R_D/r_0 \ll 1$. Therefore, a greater number of electrons are lost to the wall for a larger value of R_D/r_0. In an idealized case, it can be shown that the thrust is given by $F \propto B_z(R_D/r_0)^2$.[15,16] Thus, the thrust is expected to increase with the increase in REF strength at fixed ω and B_z up to the optimum ratio.[15,16] Therefore, the penetration of REF into dense helicon plasmas is a key issue. The gyration motion of electrons also produces j_θ (diamagnetic current). However, j_θ of the diamagnetic current is smaller than that of the current excited by REF at the optimum ratio.

Although acceleration of plasma flow has been observed in experiments,[8–12] the increase in ion velocity was argued by the increase in plasma temperature. In other words, the thermal process dominates acceleration. We note here that the optimum R_D/r_0 was not achieved in those experiments owing to the lack of theoretical works as mentioned above. A parametric survey[17] using the analytical thrust model[15,16] showed that the electromagnetic thrust by the Lissajous acceleration could dominate over the thrust by the thermal acceleration at an optimum R_D/r_0. The parameter (R_D) depends on the REF in plasma, which is an unknown parameter due to the shielding by the plasma. In order to design experiments at an optimum R_D/r_0, the REF strength in plasma should be determined prior to the experiments. Therefore, a simple theoretical model that can be used to estimate the REF strength in plasma is demanded.

In this paper, the electric field penetration into magnetized plasma is evaluated using a one-dimensional (1D) analytical model, which is the electrostatic matrix sheath model similar to that discussed in ref. 18. The electric field is obtained as the function of q, which accounts for the degree of shielding for the electric field in magnetized plasma with a cold electron fluid. The problem is also considered using the analytical vacuum gap model, where the sheaths are replaced by "effective" vacuum gaps. This model is similar to that used in refs. 9 and 11, but accounts for gap widths self-consistently, by setting them equal to an excursion length of the electron polarization drift. Both analytical models are shown to yield identical results. Finally, the problem is examined by 1D PIC simulations, and the results are found to be consistent with those obtained using the analytical models.

2. Electric Field Penetration Models

In LHPA, the electric field is a rotating vector with both the x and y components. Here, as the first-order approach to evaluate the field penetration, we consider 1D models neglecting the rotation.

2.1 Electrostatic matrix sheath model

The geometry of this model is shown in Fig. 2. A slab of neutral plasma ($n_e = n_i = n_0 =$ constant, where n_i and n_e are the ion and electron densities, respectively) is placed between two RF antennas that are powered by harmonic RF potentials $\pm(V_0/2)\sin\omega t$ and are spaced at a distance of L. There are ion sheaths ($n_i = n_0$, $n_e = 0$) of variable widths [$s_{1,2}(t)$] between the plasma and the RF antennas. The system is immersed in a uniform strength of ambient magnetic field B_z. Note that this model is similar to that used

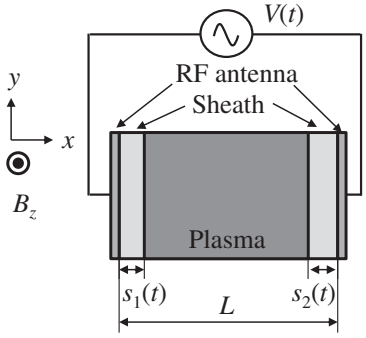

Fig. 2. Schematic of the electrostatic matrix sheath model.

in ref. 18 for capacitively coupled discharge. However, our approach differs from that in ref. 18 in that we assume that the applied potential, rather than the current, is harmonic.

To find the RF potential, one has to solve Poisson's equations: in the sheath,

$$-\frac{\partial}{\partial x}\left(\varepsilon_0\frac{\partial\phi_s}{\partial x}\right) = en_0,$$
$$-\frac{L}{2} \le x < x_1(t) \text{ and } x_2(t) < x \le \frac{L}{2}, \tag{1}$$

and in the plasma,

$$-\frac{\partial}{\partial x}\left(\varepsilon_0\frac{\partial\phi_p}{\partial x}\right) = 0, \quad x_1(t) \le x \le x_2(t), \tag{2}$$

with e and ε_0 being the electron charge and the vacuum permittivity, respectively. Here, the origin of the x coordinate is set in the middle of the RF antennas, so that the plasma boundaries are positioned at $x_1(t) = -L/2 + s_1(t)$ and $x_2(t) = L/2 - s_2(t)$. The solutions of eqs. (1) and (2) are as follows:

$$\phi_{s1}(x) = -\eta\frac{x^2}{2} + C_1x + D_1, \quad -\frac{L}{2} \le x < x_1(t), \tag{3}$$
$$\phi_{s2}(x) = -\eta\frac{x^2}{2} + C_2x + D_2, \quad x_2(t) < x \le \frac{L}{2}, \tag{4}$$
$$\phi_p(x) = A_px + B_p, \quad x_1(t) \le x \le x_2(t), \tag{5}$$

where $\eta = en_0/\varepsilon_0$. The joining conditions at plasma boundaries are the following:

$$\phi_{s1}(x_1) = \phi_p(x_1), \quad \phi_{s2}(x_2) = \phi_p(x_2), \tag{6}$$
$$\left.\frac{\partial\phi_{s1}}{\partial x}\right|_{x_1} = \left.\frac{\partial\phi_p}{\partial x}\right|_{x_1}, \quad \left.\frac{\partial\phi_{s2}}{\partial x}\right|_{x_2} = \left.\frac{\partial\phi_p}{\partial x}\right|_{x_2}. \tag{7}$$

The system of equations is closed by setting potentials of the RF antenna as a known function, $V(t)$.

$$\phi_{s1}\left(-\frac{L}{2}\right) = \frac{V(t)}{2}, \quad \phi_{s2}\left(\frac{L}{2}\right) = -\frac{V(t)}{2}. \tag{8}$$

The electric fields in the plasma and sheath take the form

$$E_p = \frac{1}{L}\left[V(t) + \eta\frac{s_1^2 - s_2^2}{2}\right], \tag{9}$$
$$E_{s1} = \eta\left(x + \frac{L}{2} - s_1\right) + E_p,$$
$$E_{s2} = \eta\left(x - \frac{L}{2} + s_2\right) + E_p. \tag{10}$$

Here, E_{s1} and E_{s2} are electric fields in the sheaths. Next, the sheath widths s_1 and s_2 are required in order to estimate the electric field.

The plasma width is found to be constant from a consideration of current conservation in the system in the following discussion. Taking the divergence of Maxwell equation in the 1D geometry leads to a conclusion that dictates that the total current is conserved in the system:

$$\nabla \cdot (\nabla \times \mathbf{H}) = \nabla\left(\mathbf{j} + \varepsilon_0 \frac{\partial \mathbf{E}}{\partial t}\right) = 0. \tag{11}$$

Therefore, the current flowing into or out of the plasma through the sheaths should be cancelled:[18]

$$\varepsilon_0 \frac{\partial E_1}{\partial t}\bigg|_{x=-L/2} = \varepsilon_0 \frac{\partial E_2}{\partial t}\bigg|_{x=L/2}. \tag{12}$$

The convection current is set at zero since no electrons are in the sheath and ions are immobile. The substitution of the electric fields from eq. (10) into eq. (12) yields

$$\frac{\partial}{\partial t}\eta(s_1(t) + s_2(t) - L) = 0. \tag{13}$$

Therefore, the width of plasma is constant for a uniform density. We further assume a harmonic motion of the sheath and a sinusoidal RF voltage drive. As shown in the Appendix, under the condition $\omega_{ce} > \omega$, the phase of the sheath motion should be set as follows:

$$\begin{aligned} s_1(t) &= s_0(1 - \sin\omega t), \\ s_2(t) &= s_0(1 + \sin\omega t), \\ V_0(t) &= V_0 \sin\omega t. \end{aligned} \tag{14}$$

Substituting eq. (14) into eq. (9) yields

$$E_p = \frac{1}{L}\left(V_0 - \frac{2ens_0^2}{\varepsilon_0}\right)\sin\omega t. \tag{15}$$

In this model, all plasma electrons move as a rigid box, as long as the plasma field, eq. (15), is coordinate-independent, i.e., uniform. Consider the motion of the electron positioned at the left plasma boundary, i.e., with the coordinate $x(t) = -L/2 + s_1(t)$ and the x-component of the velocity $v_x = ds_1/dt$. Newtonian equations of its motion take the form

$$\frac{d^2 s_1}{dt^2} = -\frac{e}{m}E_p - \omega_{ce} v_y, \tag{16}$$

$$\frac{dv_y}{dt} = \omega_{ce}\frac{ds_1}{dt}. \tag{17}$$

Here, m is the electron mass, $\omega_{ce} = eB_z/m$ is the electron cyclotron frequency, and v_y is the transverse electron velocity (similar equations can be obtained for s_2). The solution of eq. (17), with the initial condition $v_y(0)$, is $v_y = \omega_{ce}s_1 - \omega_{ce}s_0$. Substituting this v_y and eq. (9) into eq. (16) yields

$$\frac{d^2 s_1}{dt^2} = -\frac{e}{mL}\left(V_0 \sin\omega t + \frac{en}{\varepsilon_0}\frac{s_1^2 - s_2^2}{2}\right) - \omega_{ce}^2(s_1 - s_0). \tag{18}$$

Substituting eq. (14) into eq. (18) yields an equation for s_0

$$2\omega_{pe}^2 s_0^2 + (\omega_{ce}^2 - \omega^2)Ls_0 - eV(t)/m = 0. \tag{19}$$

The solution of this is

$$s_0 = \frac{L}{4}\frac{\omega_{ce}^2}{\omega_{pe}^2}(\sqrt{\varepsilon^2 + q} - \varepsilon), \tag{20}$$

where $\varepsilon = 1 - \omega^2/\omega_{ce}^2$ and

$$q = 8\frac{\omega_{pe}^2}{\omega_{ce}^2}\frac{\delta}{L}, \tag{21}$$

$$\delta = \frac{e}{m\omega_{ce}^2}\frac{V_0}{L}. \tag{22}$$

Here, the plasma frequency is given by $\omega_{pe} = (n_0 e^2/m\varepsilon_0)^{1/2}$. We consider the frequency range $\omega_{ce} \gg \omega$, thus $\varepsilon \sim 1$. Substituting eq. (20) into eq. (15), the amplitude of the electric field in the plasma is obtained as

$$\frac{E_{p0}}{V_0/L} = \frac{2\varepsilon}{q}(\sqrt{\varepsilon^2 + q} - \varepsilon). \tag{23}$$

Here, the amplitude is defined as $E_p(t) = E_{p0}\sin\omega t$. In eq. (23), V_0/L is the amplitude of vacuum electric field without plasma. The amplitude of the field monotonically decreases with the increase in q, as shown in the latter. Electric field strength is governed by the dimensionless parameter q. For $q \ll 1$, the field strength is nearly equal to the strength obtained without plasma ($E_{p0} \sim V_0/L$). For $q \gg 1$, the field is weak and scales as $E_p(t) \propto 1/\sqrt{q}$.

The parameter q represents the two following effects. The first is the shielding of the applied electric field by ion sheaths. When the total charge in the ion sheaths is large, electric field becomes weak in the plasma. When plasma density increases, the sheath width falls as $s_0 \propto 1/\sqrt{n}$ for $q \gg 1$, as seen from eq. (20) at other fixed parameters. The ion density in the sheaths grows linearly. The total charge in the ion sheaths scales as $s_0 n \propto \sqrt{n}$; therefore, the electric field is expected to become weaker. Second, when the magnetic field increases, at other fixed parameters, q decreases with the simultaneous decrease in electron mobility across the magnetic field. In consequence, sheath width decreases resulting in the weakening of the shielding effect of the sheaths and the increase in electric field within plasma.

2.2 Vacuum gap model

In this model, the configuration of the system is similar to that shown in Fig. 2, but the ion sheaths are replaced by the "effective" vacuum gaps of equal, fixed widths $s_1 = s_2 = s_g$. The vacuum gaps are determined self-consistently. The plasma is described by an electric displacement $D_x = \varepsilon_\perp E_x$, where

$$\varepsilon_\perp = 1 - \frac{\omega_{pe}^2}{\omega^2 - \omega_{ce}^2} \tag{24}$$

is a perpendicular component of the cold-plasma dielectric tensor.[19] The other field components, E_y and E_z, are assumed to be zero.

To find the fields, we solve Poisson's equation: in the sheath

$$\begin{aligned} &-\frac{\partial}{\partial x}\left(\varepsilon_0 \frac{\partial \phi_s}{\partial x}\right) = 0, \\ &-L/2 \le x < x_{1g} \text{ and } x_{2g} < x \le L/2, \end{aligned} \tag{25}$$

and in the plasma,

$$-\frac{\partial}{\partial x}\left(\varepsilon_{\perp}\frac{\partial \phi_{\mathrm{p}}}{\partial x}\right)=0, \quad x_{1\mathrm{g}} \le x \le x_{2\mathrm{g}} \tag{26}$$

where $x_{1\mathrm{g}} = -L/2 + s_{\mathrm{g}}$ and $x_{2\mathrm{g}} = L/2 - s_{\mathrm{g}}$ are the coordinates of plasma–gap boundaries. The continuity of potential and electric displacement is assumed throughout the system, and the same boundary conditions are applied as in eqs. (6) and (8), but with $x_{1,2\mathrm{g}}$ instead of $x_{1,2}$. The boundary conditions for the electric displacement are modified from eq. (7) to

$$\left.\frac{\partial \phi_{\mathrm{s1}}}{\partial x}\right|_{x_{1\mathrm{g}}} = \varepsilon_{\perp}\left.\frac{\partial \phi_{\mathrm{p}}}{\partial x}\right|_{x_{1\mathrm{g}}}, \quad \left.\frac{\partial \phi_{\mathrm{s2}}}{\partial x}\right|_{x_{2\mathrm{g}}} = \varepsilon_{\perp}\left.\frac{\partial \phi_{\mathrm{p}}}{\partial x}\right|_{x_{2\mathrm{g}}}. \tag{27}$$

Solving eqs. (25) and (26) using with the boundary conditions yields the electric field in the plasma:

$$E_{\mathrm{p}} = \frac{V(t)}{L}\frac{1}{1+2(\varepsilon_{\perp}-1)s_{\mathrm{g}}/L}. \tag{28}$$

The sheath width s_{g} is set to the amplitude of electron polarization drift excursion length, whose derivation is given as follows. Polarization drift velocity is written for our configuration as[20)]

$$v_{\mathrm{p}} = -\frac{e}{m\omega_{\mathrm{ce}}^2}\frac{dE_{\mathrm{p}}}{dt}. \tag{29}$$

Setting this velocity to be equal to sheath velocity ($ds_{\mathrm{g}}/dt = v_{\mathrm{p}}$) yields the expression for sheath width,

$$s_{\mathrm{g}} = -\frac{eE_{\mathrm{p}}}{m\omega_{\mathrm{ce}}^2}. \tag{30}$$

Under the condition ($\omega_{\mathrm{pe}} \gg \omega_{\mathrm{ce}} \gg \omega$), a similar equation to eq. (19) is obtained by substituting eq. (30) into eq. (28):

$$2\omega_{\mathrm{pe}}^2 s_{\mathrm{g}}^2 + \omega_{\mathrm{ce}}^2 L s_{\mathrm{g}} - \frac{eV(t)}{m} = 0. \tag{31}$$

In order to obtain an electric field in the plasma, the solution of eq. (31) is substituted into eq. (30) to yield

$$\frac{E_{\mathrm{pg0}}}{V_0/L} = \frac{2}{q}(\sqrt{1+q}-1). \tag{32}$$

Here, q is defined by eq. (21). Note that eq. (32) is identical to eq. (23) under the condition ($\omega_{\mathrm{ce}} \gg \omega$). Therefore, the electrostatic matrix sheath model and the vacuum gap model yield identical expressions for the electric field in the magnetized plasma in the practical parameter range ($\omega_{\mathrm{ce}} \gg \omega$). The vacuum gap model is easily extended to inhomogeneous plasmas using spatially dependent plasma dielectric tensors $\varepsilon_{\perp}(x)$ with a sheath width equal to the electron polarization drift excursion length at the plasma–gap boundary.

The vacuum gap model is similar to the one used by Bekefi in his textbook for the case of no magnetic field.[21)] In an approximation of a fixed vacuum gap width, S, Bekefi has found a "geometrical" resonance (infinite plasma field) at a driving frequency: $\omega = \omega_{\mathrm{pe}}\sqrt{2S/L}$ (geometrical resonance frequency). We found a geometrical upper hybrid resonance at a frequency of $\omega_{\mathrm{guh}} = [\omega_{\mathrm{ce}}^2 + \omega_{\mathrm{pe}}^2(2S/L)]^{1/2}$ by applying this approximation to a magnetized plasma. However, the vacuum gap model discussed above does not show any resonances because gap width is not fixed but is chosen self-consistently, equal to the electron polarization drift excursion length.

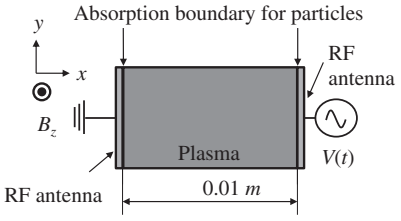

Fig. 3. Configuration of simulations.

3. PIC Simulations for Electric Field Penetration

The electric field strength obtained using the analytical model is compared with the results of 1D PIC simulations using the VORPAL code.[22)] The configuration of simulation is shown in Fig. 3. The frequency is set at $\omega/2\pi = 10$ MHz for $n_0 = 10^{17}\,\mathrm{m}^{-3}$, which is considered to be appropriate for LHPA.[16,17)] For densities of $n_0 = 10^{18}$ and $10^{19}\,\mathrm{m}^{-3}$, the driving frequency is set at 100 MHz in order to save computational time. The amplitude of potential is set at the right RF antenna, which is given as V_0 in Table I. The rise of the temporal waveform for potential is smoothed using a function [$V_0(t) = V_0 \tanh(t/\tau_0)\sin\omega t$]. The rise time of τ_0 is one-tenth of the RF period. The potential of the left RF antenna is set at zero. The distance between RF antennas is fixed at $L = 0.01$ m. The magnetic field is varied in order to change q. Table I shows the values of R_{D}/r_0, which are given by the thruster radius of $r_0 = L/2$ and eq. (32) for $E_{\perp}$. The estimated values of $E_{\perp}$ are listed as $E_{\mathrm{pg0}}/(V_0/L)$. The simulation results are shown in Table I as $|E_{\mathrm{p}}/E_0|$, which is obtained by a method described later. The numerical time step and the spatial step are set at one-tenth of plasma wave period and Debye length, respectively. The number of spatial grids is changed according to plasma density; the numbers are given in Table II. The simulation is run for 5 RF periods. Equal numbers of Ar ions with a charge state of 1 and electrons are placed in the simulation domain at the beginning of each simulation run. The ion and electron temperatures are 0.3 and 5 eV, respectively. Both energy distribution functions are assumed to be Maxwellian initially. The absorption boundary is set on the RF antenna surface for all particles. The superparticle number is fixed at 1000 per cell for simulations at a density of $10^{17}\,\mathrm{m}^{-3}$. The superparticle number per cell is varied from 200 (1,000) to 1,000 (10,000) for simulations at a density of 10^{18} (10^{19}) m^{-3}, and the results are not affected by the number of superparticles. This indicates a negligible influence of numerical heating on simulation results. We confirm that plasma density for all simulations remains practically constant and uniform during all runs. This fact ensures validity of the uniform plasma assumption.

The amplitude of electric field in the plasma at the driving frequency is compared with the theoretical curve, which is given by eq. (32) in Fig. 4. The amplitudes are also listed in Table I. Field strength is obtained from Fourier analysis for the temporal waveforms of the electric field. Electric field strength is spatially averaged over $x = 0.05L$ to $0.95L$ in order to eliminate the strong electric field in the sheath region before the Fourier analysis. The amplitude of field strength in the absence of plasma (E_0) is estimated by the

Table I. Simulation parameters I.

$\omega/2\pi$ (MHz)	V_0 (V)	B (T)	n_0 (m^{-3})	R_D/r_0	q	$\frac{E_{pg0}}{V_0/L}$	$\lvert E_p/E_0\rvert$ simulation
10	31.04	0.01	10^{17}	0.4	14.5	0.4048	0.29 ± 0.06
10	29.75	0.02	10^{17}	0.4	0.870	0.8448	0.71 ± 0.06
10	63.57	0.05	10^{17}	0.4	4.76×10^{-2}	0.9884	0.94 ± 0.10
10	125.85	0.1	10^{17}	0.4	5.89×10^{-3}	0.9985	1.01 ± 0.09
10	251.4	0.2	10^{17}	0.4	7.35×10^{-4}	0.9998	1.03 ± 0.09
10	4.296	0.01	10^{17}	0.1	2.01	0.7312	0.68 ± 0.07
10	6.572	0.02	10^{17}	0.1	0.192	0.9561	0.86 ± 0.05
10	15.75	0.05	10^{17}	0.1	1.18×10^{-2}	0.9971	0.95 ± 0.11
10	31.43	0.1	10^{17}	0.1	1.47×10^{-3}	0.9996	1.01 ± 0.09
10	62.83	0.2	10^{17}	0.1	1.84×10^{-4}	1.000	1.02 ± 0.09
10	0.3257	0.01	10^{17}	0.1	0.152	0.9645	0.74 ± 0.12
10	0.6312	0.02	10^{17}	0.01	1.85×10^{-2}	0.9954	0.83 ± 0.19
10	1.571	0.05	10^{17}	0.01	1.18×10^{-3}	0.9997	0.93 ± 0.23
10	3.142	0.1	10^{17}	0.01	1.47×10^{-4}	1.000	1.03 ± 0.04
10	6.283	0.2	10^{17}	0.01	1.84×10^{-5}	1.000	1.04 ± 0.05
100	10	0.01	10^{18}	7.15×10^{-3}	46.8	0.2527	0.12 ± 0.06
100	10	0.02	10^{18}	1.05×10^{-2}	2.92	0.6709	0.42 ± 0.02
100	10	0.03	10^{18}	9.38×10^{-3}	0.578	0.8865	0.68 ± 0.01
100	10	0.1	10^{18}	3.18×10^{-3}	4.68×10^{-3}	0.9988	0.96 ± 0.01
100	10	0.01	10^{19}	2.47×10^{-3}	4.68×10^{2}	0.08828	0.12 ± 0.04
100	10	0.03	10^{19}	5.84×10^{-3}	5.78	0.5550	0.44 ± 0.06
100	10	0.1	10^{19}	3.15×10^{-3}	4.68×10^{-2}	0.9886	0.98 ± 0.03

Table II. Simulation parameters II.

$\omega/2\pi$ (MHz)	n_0 (m^{-3})	Number of spatial grids	Number of time steps	Time step (ps)
10	10^{17}	190	14196	35
100	10^{18}	601	4489	11
100	10^{19}	1903	14196	3.5

same procedure described above. The error bar is estimated by an equation $|E(\omega_n)/E_0(\omega_0)|^2$ where the spectral noise is estimated at the frequency $\omega_n = 0.7\omega_0$. The theoretical curve of eq. (32) is also plotted in Fig. 4, and is found to be insensitive to plasma density. Estimated values from PIC simulations show a good agreement with the analytical prediction. In Fig. 4(a), the simulation results from $n_0 = 10^{17}\,\mathrm{m}^{-3}$ are shown for three values of R_D/r_0. Electric field strength decreases with the increase in q. A nearly full penetration of electric field is expected when q is smaller than 0.01 for all three values of R_D/r_0. In Fig. 4(b), the simulation results for $n_0 = 10^{18}$ and $10^{19}\,\mathrm{m}^{-3}$ are shown. Equation (32) also reproduces simulation data points for high densities.

The influence of temperature was examined for a fixed $R_D/r_0 = 0.4$ (other parameters are the same as those shown in Table I). A slight difference was observed between simulation data points for $T_e = 5\,\mathrm{eV}$ [Fig. 4(a)] and $T_e = 0.5, 50\,\mathrm{eV}$ (data not shown). The root mean square (RMS) difference from $T_e = 5\,\mathrm{eV}$ data points was ~5%. Changing ion temperature to 3 eV for $T_e = 5\,\mathrm{eV}$ showed an RMS difference of 10% (data not shown). It is unlikely that electric field penetration is affected by temperature, as determined on the basis of the results of those additional simulations.

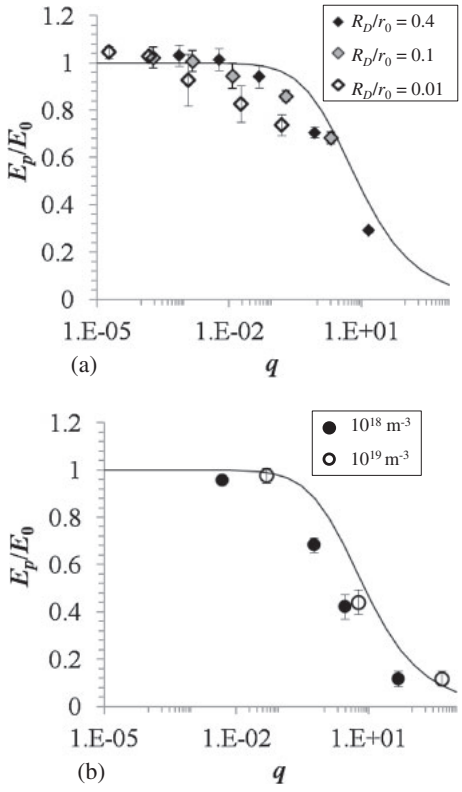

Fig. 4. Electric field strength as a function of q. (a) Simulation data points are shown for $n_0 = 10^{17}\,\mathrm{m}^{-3}$. The solid black, solid gray, and open diamonds show results for $R_D/r_0 = 0.4$, 0.1, and 0.01, respectively. (b) Simulation data points are shown for $n_0 = 10^{18}$ (10^{19}) m^{-3} by solid (open) circles. The black curves are calculated from eq. (32).

Simulation findings lead to a conclusion that the full penetration of electric field can be expected for the optimum acceleration condition ($R_D/r_0 = 0.4$) when q is kept below

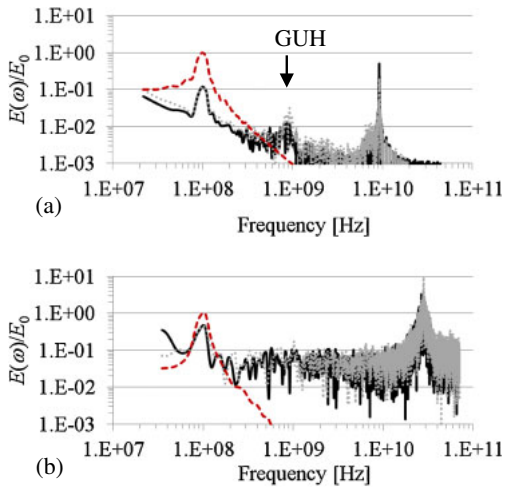

Fig. 5. (Color online) Simulated power spectra of electric field normalized by the peak value of vacuum field at the driving frequency of 100 MHz for (a) $n_e = 10^{18}\,m^{-3}$, $B = 0.01\,T$ and (b) $n_e = 10^{19}\,m^{-3}$, $B = 0.03\,T$. Other parameters are given in the text. (a) shows spectra for without plasma (red dashed), with plasma for 1,000 particles/cell (black solid), and with plasma for 200 particles/cell (gray dotted). (b) shows the spectra for the same condition as in (a) and, in addition, the case with plasma for 10,000 particles/cell (gray dotted).

0.01. This conclusion is useful for extracting scaling laws and designing experiments.

The frequency spectra of electric field in plasma are shown in Fig. 5. In all simulations, we observe two to three peaks in a spectrum. The first peak arises at the driving frequency (100 MHz), except for a data point at ($n_e = 10^{19}\,m^{-3}$, $B_z = 0.01\,T$), for which the intensity at the driving frequency is comparable to the intensity in the frequency range from 500 MHz to 1 GHz. The second peak near 10 GHz in Fig. 5(a) [near 30 GHz in Fig. 5(b)] is observed even when the RF voltage is set to zero; it is identified with normal upper hybrid resonance oscillations at the frequency $\omega_{uh} = (\omega_{ce}^2 + \omega_{pe}^2)^{1/2}$. The third peak (labeled as "GUH" in the figure) is seen in the frequency range between 600 and 900 MHz in Fig. 5(a). It is identified as the geometrical upper hybrid resonance (GUH) mentioned in §2.2, which was shown by modeling a nonstationary matrix sheath.[23] The numerical solution for the nonstationary matrix sheath model with electron collisions included, and other parameters as in Fig. 5(a), showed that the GUH resonance oscillations damp in 2–3 RF cycles. No clear GUH oscillations are observed in the simulations for a plasma density of $10^{19}\,m^{-3}$, possibly owing to a greater statistical noise than for a plasma density of $10^{18}\,m^{-3}$. The normal upper hybrid and the GUH resonance oscillations that arise at frequencies well above the driving frequency are damped owing to collisions for actual plasmas, and are thus expected to weakly influence the RF field penetration.

4. Discussion

Four issues are discussed in this section. First, the validity of the electrostatic approximation is considered. When the relation $N^2 \gg |\varepsilon_{ij}|$ is satisfied for a given parameter range, the electrostatic approximation is valid.[24] Here, N is the refractive index of plasma and ε_{ij} is the dielectric tensor of cold plasmas. We confirmed that the relation ($N^2 \gg |\varepsilon_{ij}|$) is satisfied for all simulation runs in Table I.

Second, in generating the j_θ component, a radially nonuniform plasma density is required as shown in refs. 11, 12, 15, and 16. However, in the model presented here, uniform plasmas are assumed. For a density profile peaking on the axis, the strength of REF would increase as compared with the case of a constant plasma density. This increase is due to the decrease in the plasma density at the edge of the plasma. In order to obtain an absolute value, the radial inhomogeneity should be taken into account in the present model.

Third, the collisions would influence the electric field penetration when collision frequency approaches ω for high plasma densities and/or high neutral densities. Therefore, the effect of collisions should be considered.

Fourth, the influence of finite length in the y direction is discussed. One-dimensional geometry is assumed in this paper. In the actual LHPA, the spatial dimension in the y direction is finite. A greater number of electrons could be lost to the dielectric tube than in the analysis in this paper. Relevant time scales of the problem will be compared. As is described in the introduction, an electron executes a circular motion at a radius of R_D with a frequency of ω. The electron whose trajectory intercepts the dielectric tube is lost. Therefore, the time scale of particle loss due to the $E \times B$ drift motion is the period of the RF fields. We found that the temporal waveform of a spatially averaged electric field is almost identical with that without plasma under the conditions where full penetration is observed, $|E_p/E_0| \sim 1$. This observation indicates that the time scale of the electric field penetration is much shorter than the RF period; therefore, the particle loss in the y direction unlikely affects the penetration condition. However, the electric field spatial distribution would be affected by changes in dimensions. For quantitative analysis, we need two- and three-dimensional simulations, which are beyond the scope of this paper.

5. Conclusions

In this paper, a one-dimensional RF sheath model in the electrostatic limit is developed in order to evaluate the parameter range within which a high electric field is available for LHPA. The electric field strength obtained from the model is consistent with that obtained from the 1D particle-in cell (PIC) simulations. The electric field is obtained as a function of q, which characterizes the degree of the shielding effect due to plasma density and electron magnetization. The electric field in the magnetized plasma depends on sheath width, which is found to be an excursion length of the electron polarization drift. It is found that the full penetration of electric field can be achieved for the optimum condition of LHPA when q is kept below 0.01.

Acknowledgements

This work is supported by a Grants-in-Aid for Scientific Research (S, 21226019) from the Japan Society for the Promotion of Science.

Appendix

The Newtonian motion equation of an electron in the field $E_p = E_0 \sin \omega t$ is given by

$$\frac{dv_x}{dt} = -\frac{e}{m}E_0 \sin\omega t - \omega_{ce} v_y, \tag{A·1}$$

$$\frac{dv_y}{dt} = \omega_{ce} v_x. \tag{A·2}$$

The harmonic solutions to these equations are

$$v_x = -\frac{eE_0\omega}{m(\omega_{ce}^2 - \omega^2)}\cos\omega t, \tag{A·3}$$

$$v_y = -\frac{eE_0\omega_c}{m(\omega_{ce}^2 - \omega^2)}\sin\omega t. \tag{A·4}$$

Considering that $\dot{s}_1 = v_x$, the solution for the sheath width is obtained as

$$s_1(t) = -\frac{eE_0}{m(\omega_{ce}^2 - \omega^2)}\sin\omega t + \frac{eE_0}{m(\omega_{ce}^2 - \omega^2)}. \tag{A·5}$$

Equation (A·5) can be rewritten in the form

$$s_1(t) = s_0[1 - \mathrm{sign}(\omega_{ce}^2 - \omega^2)\sin\omega]. \tag{A·6}$$

Here, we define s_0 as

$$s_0 = \left|\frac{eE_0}{m(\omega_{ce}^2 - \omega^2)}\right|. \tag{A·7}$$

The expression $\mathrm{sign}(\omega_{ce}^2 - \omega^2)$ is 1 (-1) for $\omega_{ce} > \omega$ $(\omega_{ce} < \omega)$.

1) R. G. Jahn: *Physics of Electric Propulsion* (MacGraw-Hill, New York, 1968) Chap. 1, p. 2.
2) K. Kuriki and Y. Arakawa: *Denkisuishin Roket Nyuumon* (Introduction to Electric Propulsion) (University of Tokyo Press, Tokyo, 2003) Chap. 1, p. 11 [in Japanese].
3) Y. Arakawa, H. Kuninaka, Y. Nakayama, and K. Nishiyama: *Ion Enjin niyoru Doryoku Koko* (Ion Engines for Powered Flight in Space) (Corona Publishing, Tokyo, 2006) Chap. 1, p. 10 [in Japanese].
4) Dan M. Goebel and I. Katz: *Fundamentals of Electric Propulsion: Ion and Hall Thrusters* (Wiley, Hoboken, NJ, 2008) Chap. 5, p. 225.
5) J. Gilland: AIAA-1998-3934.
6) S. Shinohara, T. Hada, T. Motomura, K. Tanaka, T. Tanikawa, K. Toki, Y. Tanaka, and K. P. Shamrai: Phys. Plasmas **16** (2009) 057104.
7) C. Charles: J. Phys. D **42** (2009) 163001.
8) K. Toki, S. Shinohara, T. Tanikawa, I. Funaki, and K. P. Shamrai: Proc. 28th Int. Electric Propulsion Conf., 2003, IEPC 03-0168.
9) K. Toki, S. Shinohara, T. Tanikawa, and K. P. Shamrai: AIAA-2004-3935.
10) K. Toki, S. Shinohara, T. Tanikawa, T. Hada, I. Funaki, K. P. Shamrai, Y. Tanaka, and A. Yamaguchi: J. Plasma Fusion Res. **8** (2009) 25.
11) K. Toki, S. Shinohara, T. Tanikawa, T. Hada, I. Funaki, Y. Tanaka, A. Yamaguchi, and K. P. Shamrai: JAXA-SP-08-013, p. 73 [in Japanese].
12) H. Nishida, S. Shinohara, T. Tanikawa, T. Hada, I. Funaki, T. Matsuoka, K. P. Shamrai, and T. Motomura: AIAA-2010-7013.
13) F. R. Chang Díaz: Sci. Am. **283** (2000) 90.
14) X. Sun, A. M. Keesee, C. Biloiu, E. E. Scime, A. Meige, C. Charles, and R. W. Boswell: Phys. Rev. Lett. **95** (2005) 025004.
15) T. Matsuoka, I. Funaki, T. Nakamura, K. Yokoi, H. Nishida, K. P. Shamrai, T. Tanikawa, T. Hada, and S. Shinohara: Plasma Fusion Res. **6** (2011) 2406103.
16) T. Matsuoka, T. Nakamura, K. Yokoi, T. S. Rudenko, I. Funaki, H. Nishida, K. P. Shamrai, T. Tanikawa, T. Hada, and S. Shinohara: Proc. Int. Symp. Space Technology and Science, 2011, ISTS2011-b-09.
17) S. Satoh, T. Matsuoka, T. Fujino, and I. Funaki: AIAA-2011-4008.
18) M. A. Lieberman and A. J. Lichtenberg: *Principles of Plasma Discharges and Materials Processing* (Wiley, Hoboken, NJ, 2005) 2nd ed., Chap. 11, p. 388.
19) T. H. Stix: *Theory of Plasma Waves* (AIP, New York, 1992) p. 7.
20) F. F. Chen: *Introduction to Plasma Physics and Controlled Fusion* (Plenum Press, New York, 1984) 2nd ed., Chap. 2, p. 39.
21) G. Bekefi: *Radiation Processes in Plasmas* (Wiley, New York, 1966) Chap. 5, p. 168.
22) http://www.txcorp.com/products/VORPAL/
23) T. S. Rudenko, K. P. Shamrai, T. Matsuoka, I. Funaki, and S. Shinohara: Annual Rep. 2011, Institute for Nuclear Research, NAS of Ukraine (Kiev, 2012) p. 105.
24) T. H. Stix: *Theory of Plasma Waves* (AIP, New York, 1992) p. 54.